Aeroacoustics Conferences
June 14-17, 2022, Southampton, UK
28th AIAA/CEAS Aeroacoustics 2022 Conference

10.2514/6.2022-3099

Numerical investigations on acoustic propagation effects for highly integrated intake ducts

P. Zimmermann*, A. Kolb†, S. Mancini‡
AIRBUS Defence and Space, 85077 Manching, Germany

K.-S. Rossignol§
German Aerospace Centre (DLR), 38108 Braunschweig, Germany

Aeroacoustic assessment of highly integrated propulsion systems is a challenging task at an early design stage and requires detailed physical understanding with validated numerical prediction capabilities. This work presents numerical studies of an UCAV configuration with a complex intake duct as a complementary analysis to measurements. The setup is based on the agile (unmanned) NATO air vehicle MULDICON UCAV (MULti-DIsciplinary CONfiguration) with an S-shaped intake duct to primarily shield the engine from radar. A laser-based sound source is modeled as monopole in the intake duct. The computation of the acoustic field is performed in the time domain with the Discontinuous Galerkin (DG) code DISCO++ developed by DLR. RANS mean flow fields are calculated with DLR's TAU solver as background flow input for the aeroacoustic noise propagation. A parametric study is conducted for the monopole sound source. Dependencies of the noise propagation on the intake mass flow rate and the ambient flow velocity are investigated by directivities and spectral characteristics.

I. Nomenclature

γ	isentropic exponent
ϑ_p	heat release
ρ_0	mean flow density
τ	retarded time
$A^j_{\alpha\beta}$	flux matrices
c_0	speed of sound
F^j_α	flux vectors
L	characteristic length scale
p	acoustic pressure
p^*	non-dimensional acoustic pressure
p'	pressure fluctuations
r	distance vector
s_α	source vector
t	time
t^*	non-dimensional time
u_α	acoustic variable vector
V_i	mean flow velocity
v_i	acoustic velocity

*Acoustics Engineer, Acoustics and Vibration Department.
†Acoustics Engineer, Acoustics and Vibration Department.
‡Acoustics Engineer, Acoustics and Vibration Department.
§Research Engineer, Technical Acoustics Branch, AIAA Senior member.

II. Introduction

ENGINE integration and the effects on noise source mechanisms are necessary to assess future agile aircraft designs in early design phases. The actual position of the propulsion system relative to the aircraft's planform directly impacts the noise sources and radiation directivities [1]. Intake and exhaust integration can cause complex propagation phenomena. Performance optimisation demands complex intake and exhaust designs under consideration of boundary layer ingestion or shielding effects. Aiming at the investigation of highly integrated propulsion systems numerical investigations are necessary. Therefore, the technological interest arise to evaluate current aeroacoustic prediction methodologies. The integration of the propulsion system requires dealing with highly curved geometrical intakes and poses great challenges for the engine design due to strong non-uniform flow. Aspects of noise mitigation have to be considered to reduce acoustic signatures. These capabilities are necessary to introduce noise as an additional parameter into multi-disciplinary design and performance assessments for effective agile air vehicles.

Acoustic scattering effects have been extensively studied in the past [2–4]. Previous work in the NATO STO AVT-233 group dealt with the aeroacoustics of engine installation for military air vehicles [5]. Acoustic shielding properties have been investigated for the SACCON UCAV (Stability And Control CONfiguration) planform. Experimental investigation using a generic sound source to quantify acoustic shielding effects by the airframe have been performed [6]. The main focus was to establish a first experimental database and the preliminary validation of aeroacoustic numerical simulation tools.

The present work was carried out in the scope of the NATO STO AVT-318 Task Group 'Low noise aeroacoustic design for turbofan powered NATO air vehicles'. As a continuation of previous research activities aeroacoustic noise prediction capabilities of engine installation effects and noise reduction technologies are applied to realistic agile vehicle designs and assessed within the group. Furthermore, acoustic wind tunnel tests are conducted to provide empiric validation databases.

The latest investigations are referred to the concurrent agile (unmanned) NATO air vehicle MULDICON (MULti-DIsciplinary CONfiguration) [7]. Based on the SACCON demonstrator the MULDICON design has been developed in AVT-251. It represents an advanced UCAV (Unmanned Combat Aerial Vehicle) concept with a highly integrated propulsion system, as it is shown in Fig. 1. The MULDICON version investigated in the following is referenced as DLR-F24 MULDICON UCAV. The S-shaped intake duct is the result of a design study with the primary objective of shielding the engine from radar [8]. With the effect of engine noise shielding the integrated design can imply benefits regarding low noise technologies. Fan tone shielding and noise scattering of the MULDICON intake were numerically investigated by Proskurov with a Discontinuous Galerkin method for different frequency modes [1].

In order to validate the numerical methods a modular acoustic wind tunnel model of the MULDICON with a wing span of 2 m was manufactured. Installed pipe systems enable intake mass flow rates up to 0.9 kg/s and exhaust mass flow rates up to 1.8 kg/s. Optical ports allow the generation of non-intrusive point-like sound sources in the intake duct using a pulsed laser system. Such laser-based sound sources have been studied in the past and applied in wind tunnel measurements [9, 10]. The sources are characterized by a monopole-like behavior with broadband properties and an approximately uniform directivity.

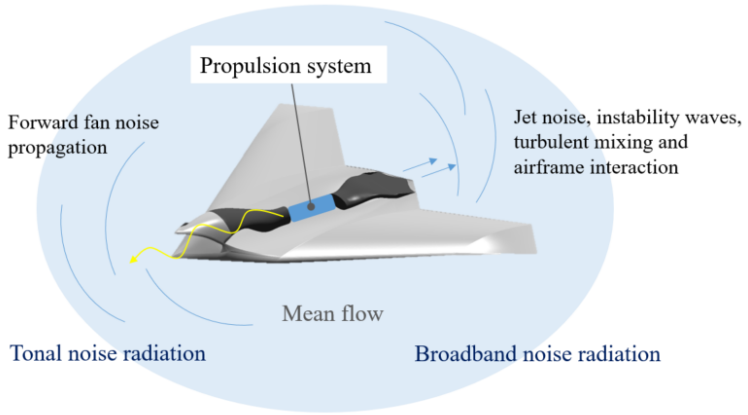

Fig. 1 Aeroacoustic aspects of the MULDICON with a highly integrated propulsion system.

The acoustic wind tunnel measurements of the MULDICON intake are presented by Rossignol et al. in a companion paper. The present work deals with CAA calculations of the source modeling and wave propagation for the given intake duct geometry.
Beginning with an overview of the numerical setup derived from the wind tunnel experiments the following Sec. III describes the boundary conditions and assumptions as well as numerical methods and processes. The results of this work are presented in Sec. IV. First, the mean flow input for the aeroacoustic simulations is assessed. Second, a parameter study of the pulse sound source without background flow is shown. The subsequent results including background mean flow and the pulse sound source give dependencies on the ambient wind tunnel velocity and the intake air suction. The findings are summarized in Sec. V.

III. Assumptions and Processes

The numerical framework is derived from wind tunnel measurements of the MULDICON intake in the low speed acoustic facility Braunschweig (NWB) described by Rossignol et al. in a companion paper. The experimental setup with the installed MULDICON model is shown in Fig. 2 (left). The demonstrator is mounted on the upper side on two struts that cover the pipes for the intake air suction. The two suction pipes are connected to the intake duct via a T-junction that is shown in Fig. 2 (right). The two circular interfaces between the T-junction and the suction pipes represent the intake zones for the mean flow calculations.
The numerical models correspond to simplified setups. The aerodynamic and aeroacoustic investigations are based on free-field conditions. Regarding the mean flow calculations the wind tunnel environment is considered to be negligible for the low angle of attacks in the vicinity of the aircraft.
The present work is focused on ambient free stream velocities of up to Ma 0.117 and intake mass flow rates up to 0.4 kg/s. The free stream velocity is referred to the velocity achieved at the wind tunnel nozzle exit. Tripping at 5% chord was used in the experiment on the suction and pressure side.

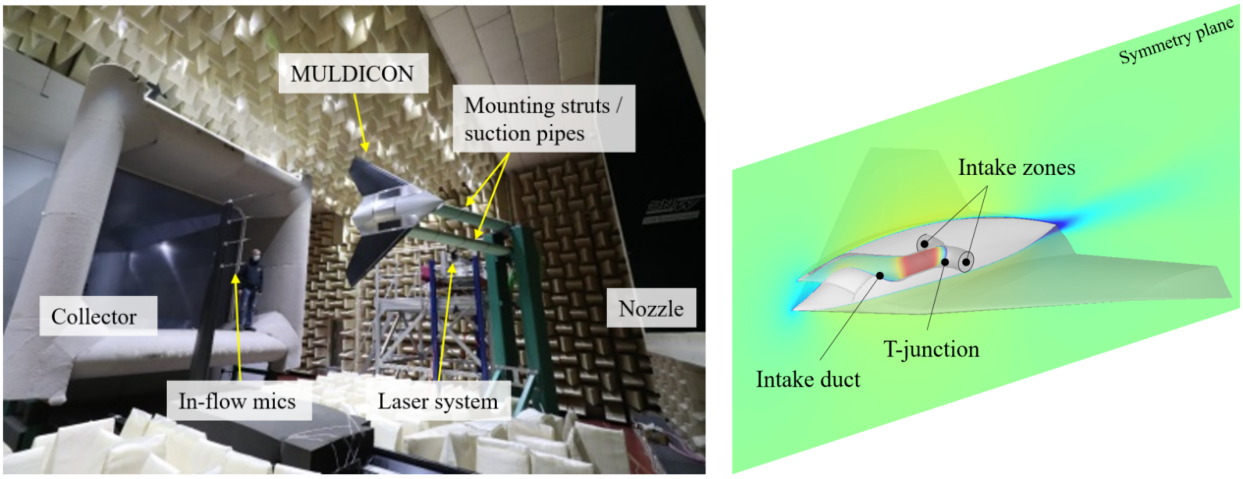

Fig. 2 Experimental setup in the low speed wind tunnel Braunschweig by DLR (left) and numerical MULDICON model with highlighted intake interfaces (right).

A. Tool chain and numerical methods

The numerical tools applied in the present work comprise computational fluid dynamics (CFD) and computational aeroacoustics (CAA) solvers as it is outlined in Fig. 3. As an interface between both the mean flow results are interpolated from the CFD grid to the CAA grid. The background mean flow is calculated on an unstructured mesh with DLR's TAU solver using the Reynolds-averaged Navier-Stokes equations (RANS). As turbulence model the k-ω Menter SST model is used with central flux discretization and scalar dissipation.
The computation of the acoustic field is performed in the time domain with the Discontinuous Galerkin (DG) code

DISCO++ developed by DLR [11–13]. It solves the linear acoustic perturbation equations (APE) on three dimensional tetrahedral grids by a quadrature-free DG method. The explicit fourth-order Runge–Kutta scheme is used for time integration. The laser-based sound source from the measurements is modeled with a monopole as subsequently described. The acoustic waves are extrapolated to the far field according to the Ffowcs-Williams Hawkings method (FW-H).

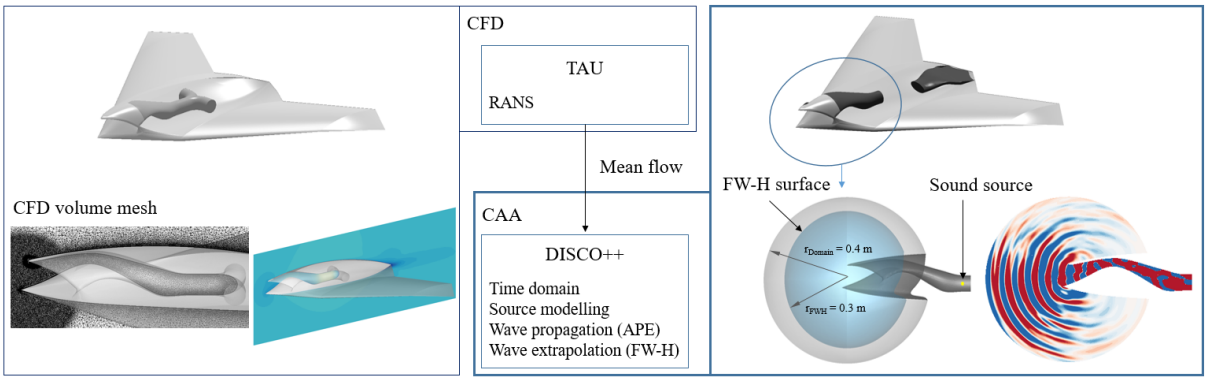

Fig. 3 Numerical process and setups.

B. Numerical model and boundary conditions

The mesh for the RANS calculations consists of an spherical domain with a radius of 100 m and about 93 million cells. The area of the intake as well as the leading edges and intake lips are additionally refined, see Fig. 3 (left). The boundary layer on the MULDICON is resolved with 30 prism layers to obtain $y^+ \leq 1$. Viscous wall effects are considered for the surfaces of the MULDICON including the intake duct. The intake zones of the T-junction are modeled as engine intakes defined by a mass flow rate. The total mass flow rate corresponds to the sum through both zones. The ambient flow velocities and mass flow rates are derived from the measurements. In contrast to the experimental setup the MULDICON is simulated in free-field conditions without mounting struts attached to it. Furthermore, the numerical geomentry has no exhaust opening on the upper rear side as the focus lies on the intake. The influence of the exhaust on the flow field around the intake is considered to be negligible.

The acoustic domain includes the MULDICON intake with a spherical boundary of 0.4 m radius as it is shown in Fig. 3 (right). The permeable Ffowcs-Williams Hawkings surface represents an offset with a radius of 0.3 m. Microphones are defined on circles around all three axis in 1 m distance to the lower intake tip with a spacing of 1 deg. The mesh cell size is chosen to resolve a maximum frequency of 10 kHz. Slip wall boundary conditions are assigned to the intake surfaces setting the wall-normal fluctuations to zero. The position of the monopole sound source is taken from the measurements and lies in the center of the circular duct section. The axial distance to the intake tip amounts 0.58 m. Since only the intake geometry is considered in the CAA domain scattering effects around the vehicle are not investigated. The calculations are conducted with a time step of $1.17e$-7 s for a total of $5e5$ s steps corresponding to 0.058 s of total computed time. The captured time signals of the acoustic pressure fluctuations are postprocessed using a Fast Fourier Transform (FFT) with a Hanning window function and a window overlap of 0.5.

C. Wave propagation model

The DG code used for this work solves the linear acoustic perturbation equations that can be written in matrix vector notation as [11, 14]

$$\partial_t u_\alpha + F^j_{\alpha,j} - s_\alpha = 0 \tag{1}$$

with the acoustic variable vector $u_\alpha = (p v_i)^\top$ including the acoustic pressure p and velocity v_i. The source vector s_α represents the pressure and momentum equations of the source. The flux vectors $F^j_\alpha = A^j_{\alpha\beta} u_\beta$ contain the mean flow

velocity V_i, density ρ_0 and speed of sound c_0 whereby $A^j_{\alpha\beta}$ can be formulated as [11]

$$A^0_{\alpha\beta} = \begin{pmatrix} V_0 & \rho_0 c_0^2 & . & . \\ \frac{1}{\rho_0} & V_0 & V_1 & V_2 \\ . & . & . & . \\ . & . & . & . \end{pmatrix}, A^1_{\alpha\beta} = \begin{pmatrix} V_1 & . & \rho_0 c_0^2 & . \\ . & . & . & . \\ \frac{1}{\rho_0} & V_0 & V_1 & V_2 \\ . & . & . & . \end{pmatrix}, A^2_{\alpha\beta} = \begin{pmatrix} V_2 & . & . & \rho_0 c_0^2 \\ . & . & . & . \\ . & . & . & . \\ \frac{1}{\rho_0} & V_0 & V_1 & V_2 \end{pmatrix}. \quad (2)$$

The indices $0-2$ indicate space indices and α, β variable indices. The dots stand for zeros.

D. Intake noise source

The numerical source model can be traced back to previous studies with similar setups [2, 15]. The mechanism of the laser-based source is described by the formation and expansion of plasma due to the energy input generating a pear-shaped pressure wave. After forming an idealized sphere of approximately 10 mm radius the pressure front propagates as an isentropic acoustic wave. The source shows monopole-like characteristics with an approximately uniform directivity and broadband behavior. An analytical model for the heat release function $\vartheta_p(\tau)$ was derived from the acoustic wave equations [16]:

$$\vartheta_p(\tau) = \frac{c_0^2 4\pi}{\gamma - 1} \int_{\tau_L}^{\tau} r_0^+(\tau) p^{'}(x, t(\tau)) d\tau. \quad (3)$$

Thereby, τ corresponds to the retarded time and r_0^+ to the distance the sound signal travelled with regard to the medium at the time of reception. It has been shown that the analytical model matches with approximated temporal Gaussian functions.

The numerical sound source used in the following is a monopole that is referred to a heat source specified by a pressure impulse. The spatial distribution is approximated by a Gaussian function with a spatial half width of 10 mm. With a cell size of about 5 mm in the CAA domain the half width is resolved with 2 cells. The temporal behavior is modeled by a Gaussian function defined by a peak time, half width and amplitude. The temporal half width specifies the time interval between the maximum and half the value. A non-dimensional temporal half width of $5.15e$-3 and a peak time of $10.30e$-3 for reaching the maximum is set as reference. The non-dimensional pressure amplitude amounts 0.157. The pressure p is given in non-dimensional notation p^* referring to the ambient density ρ_0 and the ambient speed of sound c_0, $p^* = \frac{p}{\rho_0 c_0^2}$. The non-dimensional time t^* is given by $t^* = t\frac{c_0}{L}$ with a characteristic length scale L. The Gaussian values are derived from source measurements in the Aeroacoustic Wind Tunnel Braunschweig (AWB) at DLR. The pulsed sound sources in the experiments were generated with a repetition rate of 10 Hz. The numerical calculations refer to a single pulse. In order to determine the sensitivity of the Gaussian parameters on the simulation results several variations are investigated.

IV. Numerical Results

In the following sections the outcomes of the numerical studies are presented as a basis for future comparisons with the experimental results of the acoustic wind tunnel measurements. Beginning with the mean flow results of the RANS calculations the flow field in the intake is discussed for different ambient flow velocities and intake mass flow rates. Subsequently, the monopole sound source is analyzed by a parametric study. The intake noise propagation depending on the intake mass flow rate is assessed in section IV.C considering the reference sound source and the background flow. The dependency of the acoustic installation effects on the ambient flow velocity at a constant intake mass flow rate is shown as final step.

A. Mean Flow

The integration of the MULDICON propulsion system leads to a complex intake duct geometry with varying cross sections. The design was assessed by considering total pressure losses, pressure distortion and swirls [16].
The background flow fields for the CAA calculations are computed for intake mass flow rates of 0.3 and 0.4 kg/s and ambient flow Mach numbers of 0, 0.087 and 0.117. The results of the velocity fields in the symmetry plane of the MULDICON are shown in Fig. 4. The duct cross sections at the top of the intake bump (I) and at the position of the

sound source (II) are given additionally. The vectors visualize the planar velocity field in the respective cross sections.

The velocity fields at mass flow rates of 0.3 and 0.4 kg/s without ambient flow indicate the acceleration of the fluid at the entry of the intake. The first cross sections show lower velocities at the sides in areas of stronger duct curvature. The velocity vectors outline swirled flows close to that areas. Perturbations are already observed at the lateral intake entry lips upstream of the first cross section. On the inner side of the intake bump the duct cross section changes into a more oval shape and finally into a circular form. As the second cross section in Fig. 4 shows the flow downstream of the geometrical transition is influenced by two counter-rotating vortices. Smaller circulation areas can be observed below the main vortices. The fluid gets accelerated to a maximum reaching the circular duct section. The flow characteristics between the mass flow rate of 0.3 and 0.4 kg/s without ambient flow show similarities with generally higher Ma numbers in the intake for 0.4 kg/s. As the T-junction is not part of the CAA domain this area is not discussed in detail.

The RANS results at ambient flow Mach numbers of 0.087 and 0.117 are given in Fig. 4 for a mass flow rate of 0.4 kg/s. In contrast to the cases without ambient flow the entry flow direction at the lateral intake lip is dominated by the ambient flow. Therefore, no significant flow perturbations can be observed. The flow velocity increases towards the top of the intake bump. The velocity vectors in the first cross section indicate a more uniform flow compared to the results without ambient flow. The flow velocity decreases on the lower inner side of the duct before getting accelerated towards the circular section. The vectors in the circular cross section show two small symmetric vortices at the bottom for both Ma 0.087 and 0.117.

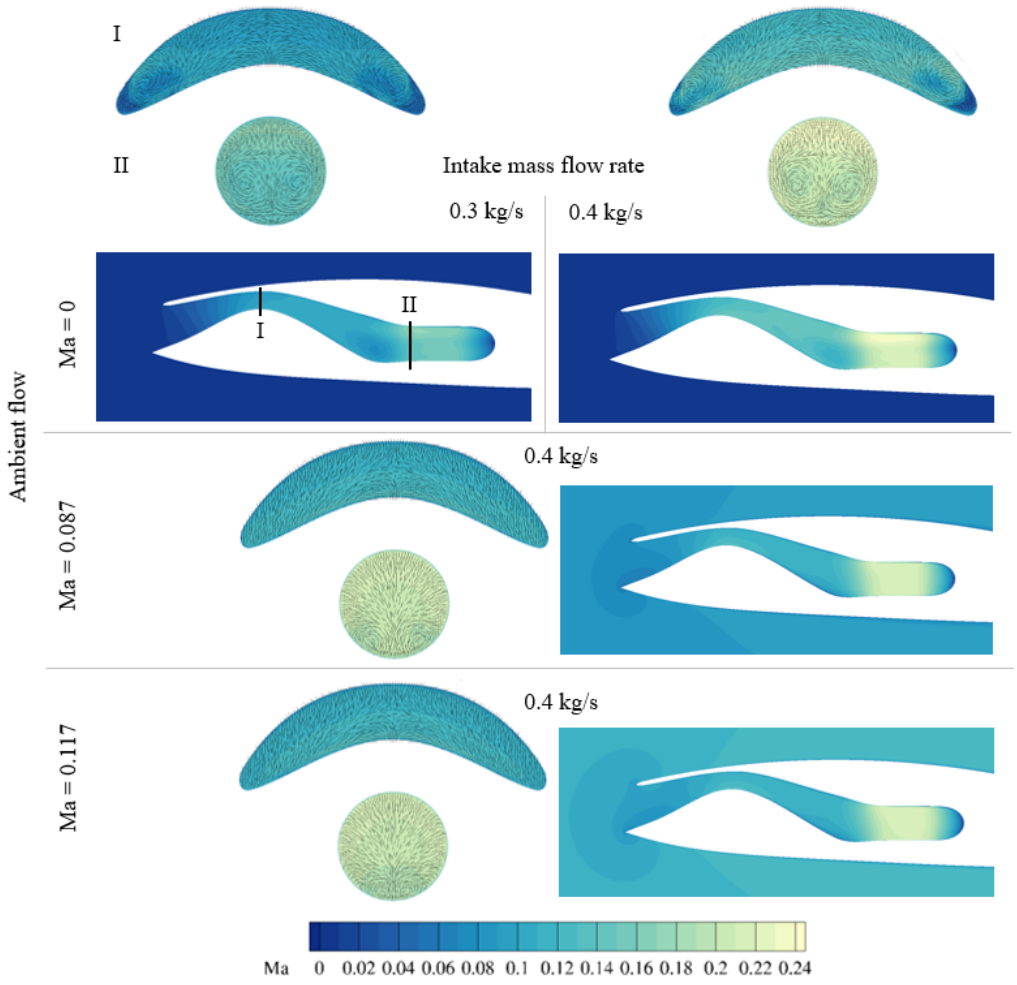

Fig. 4 Mean flow results for ambient flows of Ma=0, Ma=0.117 and intake mass flow rates of 0.3 kg/s, 0.4 kg/s.

B. Gaussian pulse source modeling

The first step in the acoustic analysis refers to the point-like sound source. As stated in Sec. III.D it is modeled as monopole defined by a spatial and temporal Gaussian function. The mentioned Gaussian parameter values correspond to the reference pulse. In order to identify the sensitivity of these parameters on the wave propagation and installation effects a parametric study is conducted. Therefore, the spatial half width, the temporal half width and the peak time are doubled in separate calculations, respectively. The other values correspond to the reference values.
The characteristics of the different pulses can be seen in Fig. 5. The graph shows the temporal pressure fluctuation received at a microphone in 0.2 m distance to the source in a free-field without duct geometry. The solid line correspond to the reference parameters. Doubling the spatial half width (HW) leads to a pressure amplitude that is approximately a quarter of the reference pulse. As the spatial half width defines the distribution of the source in space an increase of it distributes the constant energy input over a larger volume. That entails lower local amplitudes of pressure fluctuations. The pulse signal with the doubled temporal half width (HT) shows on the one side a longer signal length. On the other side the amplitude is slightly higher than two times the reference amplitude. The longer time signal results in a higher energy input by what the higher amplitude can be explained. A similar behavior can be observed for doubling the peak time whereby the amplitude at 0.2 m from the source is significantly higher than the reference. As for the temporal half width increasing the peak time describes a longer time signal and higher energy input.

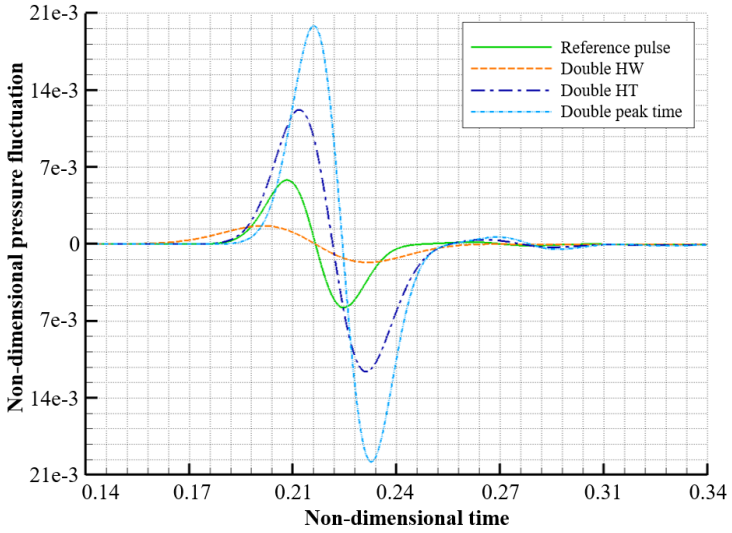

Fig. 5 Pulse signals at a distance of 0.2 m from the source in free-field conditions without duct geometry for a variation of Gaussian parameters.

The next step in the source analysis is the actual wave propagation through the MULDICON intake. With the numerical setup described in section III.B the radiated waves are captured by the Ffowcs-Williams Hawkings surface and extrapolated to the microphones in 1 m distance. The time signals are postprocessed using a Fast Fourier Transform (FFT) with a Hanning window function and a window overlap of 0.5. The results of the directivity in the symmetry plane are given in Fig. 8 as sound pressure levels (SPL) in dB for different frequencies. Additionally to the Gaussian parameters the location of the monopole is varied by offsetting it a half of the duct radius in positive z-direction. In general, the characteristics of the directivities with the Gaussian parameter variation show similarities with different magnitudes in SPL. The case with the doubled spatial half width shows lower SPL values for all given frequencies compared to the reference whereby the differences increase with the frequency. In accordance with the provided pulse signals in Fig. 5 the SPL values for the doubled temporal half width and peak time lie higher than the reference pulse for the given frequencies. Furthermore, the results of the monopole offset reveal an apparent impact on the wave radiation. While the SPL values match with the reference at 1 kHz differences can be observed at other frequencies.

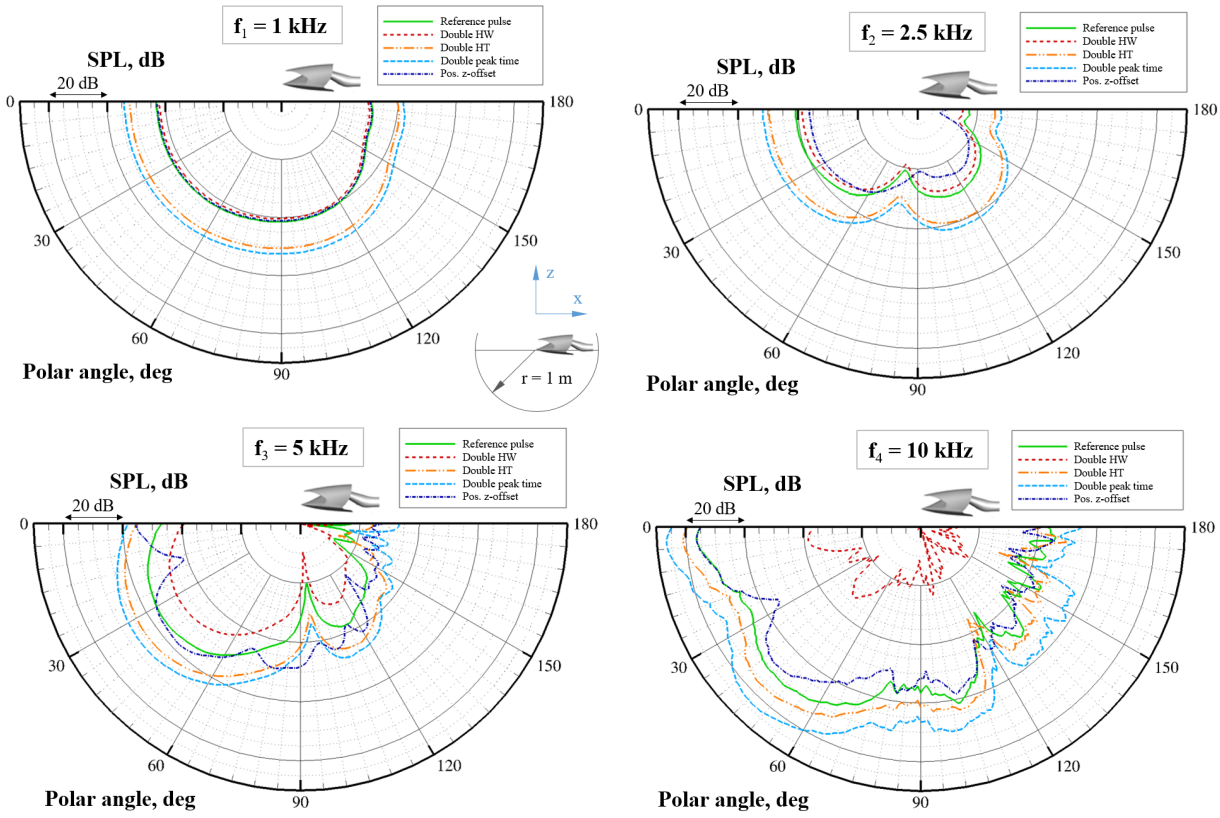

Fig. 6 Directivity of the intake noise radiation with a source parameter variation in 1 m distance.

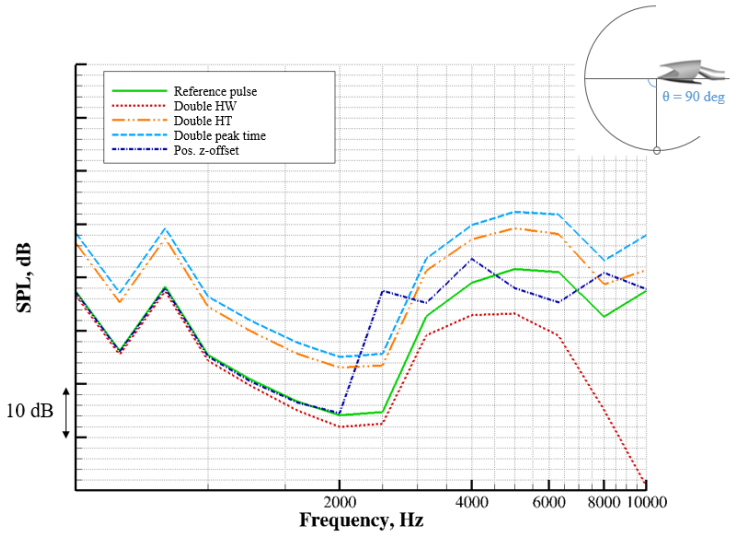

Fig. 7 SPL spectra in 1/3-octave bands of the intake noise radiation with a Gaussian source parameter variation at a 90 deg microphone in 1 m distance.

To get a better overview of the frequency content of the radiated noise a 1/3-octave band spectrum is plotted in Fig. 7 for a microphone 90 deg below the intake. The 1/3-octave bands for the case with doubled spatial half width nearly coincide with the reference pulse below 1 kHz. However, the decay above 5 kHz creates a significant gap compared to the reference. The monopole offset shows matching SPL values with the reference for frequency bands under 2 kHz. The apparent rise in SPL for the reference pulse above 2.5 kHz is shifted to a lower frequency band for the source offset. Overall, doubling the peak time leads to a rise in SPL over the given frequencies by 10-12 dB.

C. Dependency on intake suction

In the following, the results with varying intake mass flow rates are presented. No ambient flow is considered. The reference pulse is used in all computations. To investigate the influence of the intake suction on the wave propagation and radiation mass flow rates of 0.3 and 0.4 kg/s are analyzed. The results of the reference pulse without intake suction were already described in the previous section and are repeated here as reference. The directivities at 1 kHz, shown in Fig. 7, indicate a homogeneous characteristic in the forward direction 0-90 deg with slightly increasing SPL for higher mass flow rates. The SPL differences lie below 1 dB. A similar tendency can be seen for 2.5 kHz with a decrease in SPL between 45-90 deg. At higher frequencies a dominating behavior in SPL can be observed for the reference case without intake suction in the forward direction exceeding the levels with intake suction. The maximum levels lie between 25-45 deg at 5 kHz. At 10 kHz no uniform main radiation direction is given with maxima between 0-10 deg. Thereby, no consistent tendency is apparent for the mass flow rates of 0.3 and 0.4 kg/s. While the SPL values at 0.4 kg/s dominate between 0-40 deg the mass flow rate of 0.3 kg/s shows higher values in the rearward direction.

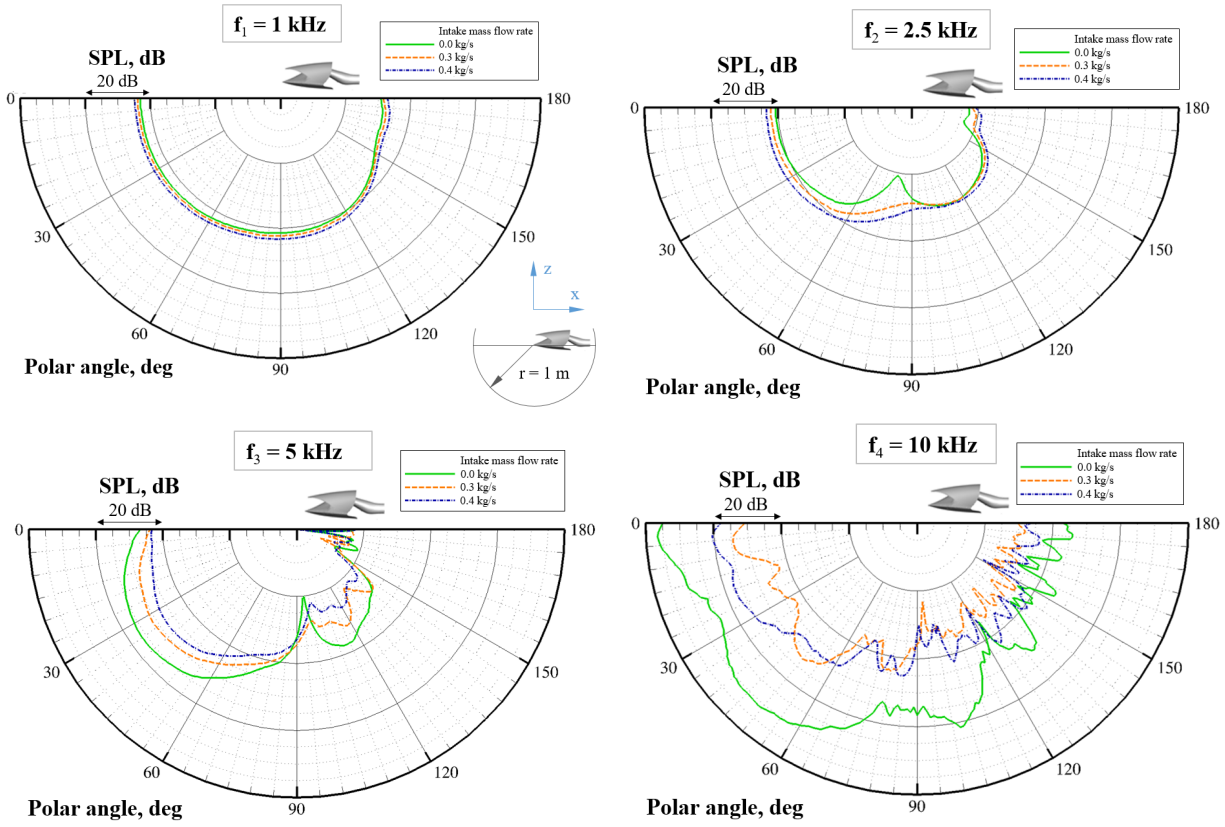

Fig. 8 Directivity of the intake noise radiation with a dependency on the intake mass flow rate without ambient flow in 1 m distance.

In contrast to Fig. 8 the trend of the 1/3-octave bands under 2 kHz, shown in Fig. 9, indicates increasing SPL for decreasing mass flow rates. The different tendency in the directivity can be explained by oscillations in the narrowband

spectrum. The 1/3-octave bands reach a minimum in noise levels at 2 kHz. Above that frequency band the results with intake suction show no clear trend regarding the SPL differences. Apart from the frequency band of 2.5 kHz the case without intake suction dominates in SPL. The maximum noise levels lie at 5 kHz for all cases.

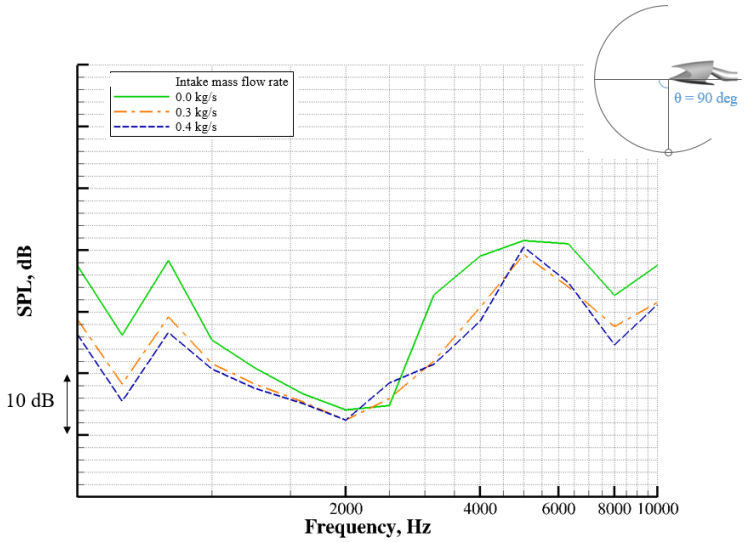

Fig. 9 SPL spectra in 1/3-octave bands of the intake noise radiation with a dependency on the intake mass flow rate without ambient flow at a 90 deg microphone in 1 m distance.

D. Dependency on ambient flow and intake suction

The mean flow results in section IV.A demonstrated the influence of the ambient flow on the mean flow field in the duct. For this reason, the acoustic installation effects are investigated for ambient flow Mach numbers of 0, 0.087 and 0.117 at a constant intake mass flow rate of 0.4 kg/s. The computation without ambient flow at 0.4 kg/s is taken from the previous section as reference. The directivities for Ma 0.087 and Ma 0.117 show no significant differences for lower frequencies, see Fig. 9. At 1, 2.5 and 5 kHz the SPL values of both cases deviate by less than 1 dB. All three cases show uniform directivities in the forward direction at 1 kHz whereby the reference without ambient flow differs by less than 2 dB. For higher frequencies the characteristic of the investigated cases show similarities with larger differences for certain angles.

The 1/3-octave band spectrum at the 90 deg microphone in Fig. 11 indicates coinciding noise levels for Ma 0.087 and Ma 0.117 in all given frequency bands. The case without mean flow reaches a maximum in the frequency band of 5 kHz with the highest difference to the other cases.

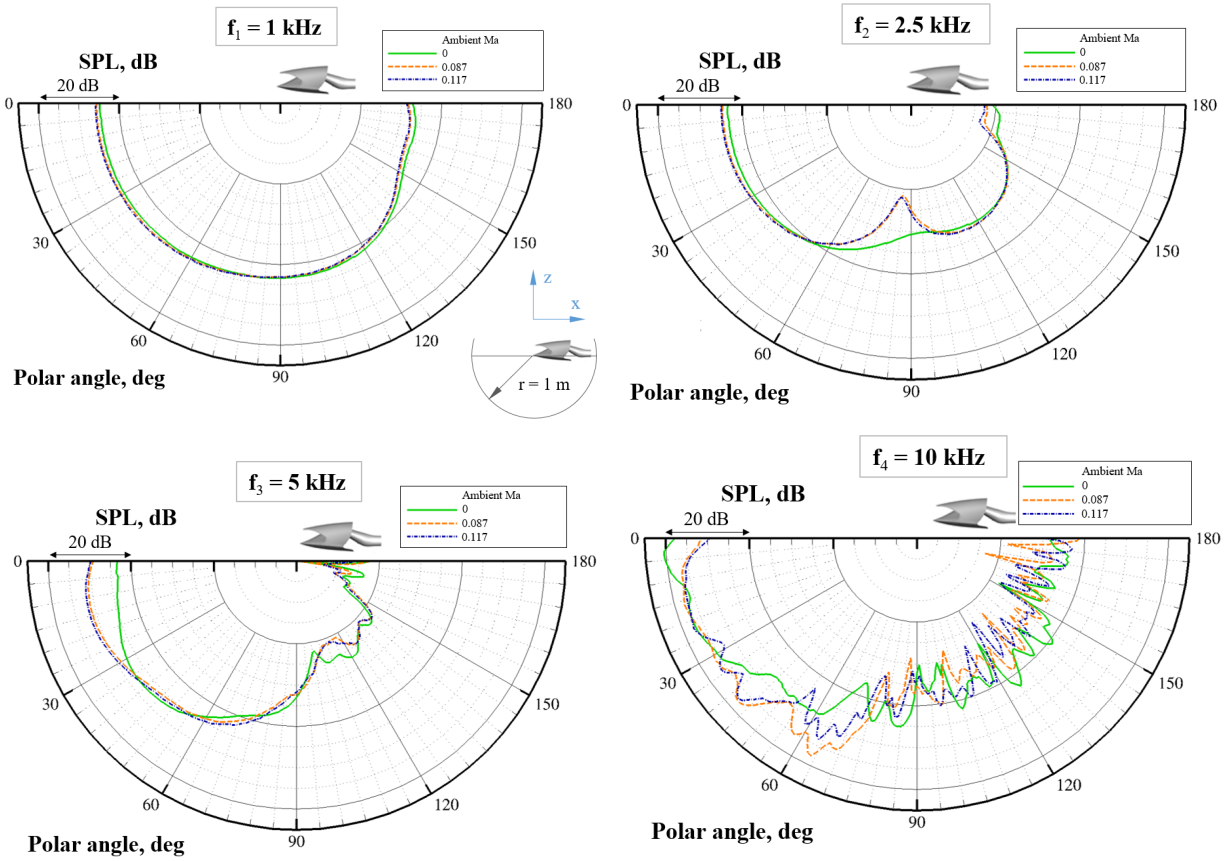

Fig. 10 Directivity of the intake noise radiation with a dependency on the ambient velocity for an intake mass flow rate of 0.4 kg/s in 1 m distance.

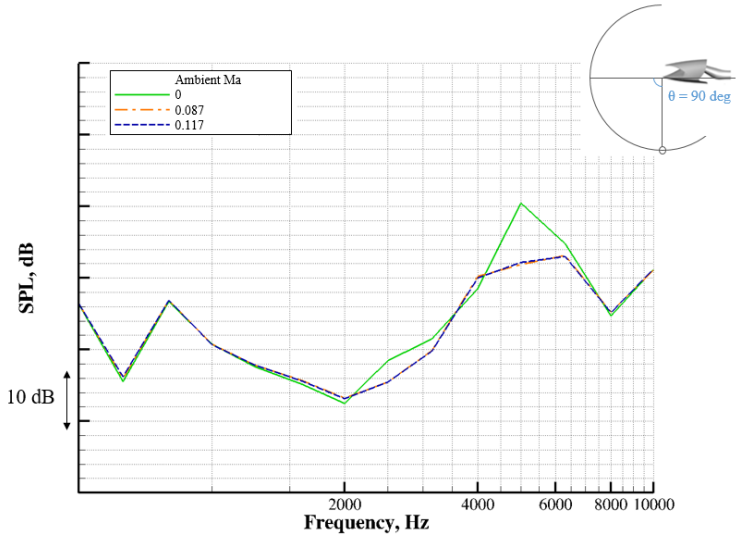

Fig. 11 SPL spectra in 1/3-octave bands of the intake noise radiation with a dependency on the ambient velocity for an intake mass flow rate of 0.4 kg/s at 45 deg and 90 deg microphones in 1 m distance.

V. Conclusion

Numerical aeroacoustic studies on noise propagation effects of a complex intake duct were presented. This work constitutes a complementary analysis to measurements that have been conducted in the low speed acoustic facility Braunschweig (NWB) at DLR. The setup is based on the agile (unmanned) NATO air vehicle MULDICON UCAV (MULti-DIsciplinary CONfiguration) with an S-shaped intake duct. In the scope of the numerical investigations a laser-based sound source was modeled in the intake duct as a monopole with spatial and temporal Gaussian functions. The computation of the acoustic field was performed in the time domain with the Discontinuous Galerkin (DG) Code DISCO++ developed by DLR. RANS mean flow fields were calculated with DLR's TAU solver as background flow input for the aeroacoustic wave propagation.

A parametric study was conducted for the monopole sound source. The influence of the energy input of the sound source on the radiated noise levels was analyzed. The computations demonstrated the sensitivity on the source position. Furthermore, dependencies of the noise propagation on the intake mass flow rate and the ambient flow velocity were investigated.

Acknowledgments

The authors would like to thank all partners of the AVT-318 Task Group.

References

[1] Proskurov, S., Mößner, M., Ewert, R., Lummer, M., and Delfs, J. W., "Fan noise shielding predictions with a coupled DG / FM-BEM method for installed aircraft engines," *AIAA AVIATION FORUM*, 2021.

[2] Rossignol, K.-S., and Delfs, J. W., "Analysis of the noise shielding characteristics of a NACA0012 2D wing," *22th AIAA/CEAS Aeroacoustics Conference*, 2016.

[3] Hutcheson, F. V., Spalt, T. B., Brooks, T. F., and Plassman, G. E., "Airframe noise from a hybrid wing body aircraft configuration," *22nd AIAA/CEAS Aeroacoustics Conference*, 2016.

[4] Papamoschou, D., and Mayoral, S., "Experiments on shielding of jet noise by airframe surfaces," *15nd AIAA/CEAS Aeroacoustics Conference*, 2009.

[5] Rossignol, K.-S., Delfs, J. W., Mößner, M., Gély, D., Bulté, J., and Hutcheson, F., "Experimental investigations on noise shielding: Dependency on reference noise source and testing environment," *24th AIAA/CEAS Aeroacoustics Conference*, 2018.

[6] Rossignol, K.-S., Proskurov, S., Lummer, M., Ewert, R., Delfs, J. W., Kolb, A., and Mancini, S., "Aeroacoustic assessment of low-observable UCAV configurations," *AVT-324 Specialists' Meeting*, 2020.

[7] Cummings, R. M., Liersch, C. M., and Schütte, A., "Multi-disciplinary design and performance assessment of effective, agile NATO air vehicles," *Applied Aerodynamics Conference*, 2018.

[8] Edefur, H., Tormalm, M., Tysell, L., and Quas, M. J., "Design and integration of a low observable intake for the MULDICON platform," *Applied Aerodynamics Conference*, 2018.

[9] Bahr, C. J., Zawodny, N. S., Bertolucci, B., Li, J., Sheplak, M., and Cattafesta, L. N., "A plasma-based non-intrusive point source for acoustic beamforming applications," *Journal of Sound and Vibration*, Vol. 344, 2015, p. 59–80.

[10] Rossignol, K.-S., Lummer, M., and Delfs, J. W., "Validation of DLR's sound shielding prediction tool using a novel sound source," *15th AIAA/CEAS Aeroacoustics Conference*, 2009.

[11] Lummer, M., "A hybrid 3D discontinuous Galerkin code for CAA applications," *22nd AIAA/CEAS Aeroacoustics Conference*, 2016.

[12] Bauer, M., Dierke, J., and Ewert, R., "On the performance of airframe noise prediction on unstructured grids," *18th AIAA/CEAS Aeroacoustics Conference*, 2012.

[13] Bauer, M., Dierke, J., and Ewert, R., "Application of a discontinuous Galerkin method to discretize acoustic perturbation equations," *AIAA JOURNAL*, Vol. 49, No. 5, 2011.

[14] Ewert, R., and Schröder, W., "Acoustic perturbation equations based on flow decomposition via source filtering," *Journal of Computational Physics*, Vol. 188, 2003, p. 365–398.

[15] Lummer, M., "Computation and validation of acoustic shielding at realistic aircraft configurations," *24th AIAA/CEAS Aeroacoustics Conference*, 2018.

[16] Rossignol, K.-S., Delfs, J. W., and Boden, F., "On the relevance of convection effects for a laser-generated sound source," *21th AIAA/CEAS Aeroacoustics Conference*, 2015.